Unravelling the elusive antiferromagnetic order in wurtzite and zinc blende CoO polymorph nanoparticles

Alejandro G. Roca, IgorV. Golosovsky, Elin Winkler, Alberto López-Ortega, Marta Estrader, Roberto D. Zysler, María Dolors Baró, Josep Nogués**

Dr. A.G. Roca, Dr. M. Estrader†, Prof. J. Nogués
Catalan Institute of Nanoscience and Nanotechnology (ICN2), CSIC and The Barcelona Institute of Science and Technology, Campus UAB, Bellaterra, E-08193 Barcelona, Spain.
†Present address: LPCNO, Université de Toulouse, CNRS, INSA, UPS, 135 avenue de Rangueil, 31077 Toulouse, France
E-mail: alejandrogroca@gmail.com, Josep.Nogues@uab.cat

Dr. I.V. Golosovsky
National Research Center "Kurchatov Institute", B.P. Konstantinov, St. Petersburg Nuclear Physics Institute, 188300 Gatchina, Russia

Dr. E. Winkler, Prof. R.D. Zysler
Centro Atómico Bariloche, CNEA-CONICET, 8400 S.C. de Bariloche, Río Negro, Argentina

Dr. A. López-Ortega
CIC nanoGUNE, Tolosa Hiribidea, 76 E-20018 Donostia-San Sebastian, Spain.

Prof. M.D. Baró
Departament de Física, Universitat Autònoma de Barcelona, 08193 Bellaterra, Cerdanyola del Vallès, Spain

Prof. J. Nogués
ICREA, Pg. Lluís Companys 23, E-08010 Barcelona, Spain

Keywords: CoO wurtzite, CoO zinc blende, antiferromagnets, incommensurate structures, uncompensated spins

Although cubic rock salt-CoO has been extensively studied, the magnetic properties of the main nanoscale CoO polymorphs (hexagonal wurtzite and cubic zinc blende structures) are rather poorly understood. Here we present a detailed magnetic and neutron diffraction studies on zinc blende and wurtzite CoO nanoparticles. The zinc blende-CoO phase is antiferromagnetic with a 3rd type structure in a fcc lattice and a Néel temperature of T_N(zinc-blende) ~ 225 K. Wurtzite-CoO also presents an antiferromagnetic order, T_N(wurtzite) ~ 109 K, although much more complex, with a 2nd type order along the c-axis but an incommensurate order along the y-axis. Importantly, the overall magnetic properties are

overwhelmed by the uncompensated spins, which confer the system a ferromagnetic–like behavior even at room temperature.

1. Introduction

In bulk, the equilibrium phase of transition metal mono-oxides of magnetic ions (CoO, NiO, FeO, MnO) is the cubic rock-salt structure.[1] However, given the key role of the surface energy[2] at the nanoscale and the strong 3d electron correlations[3] other polymorphs can become stable. For example, in CoO two new structures were reported in the 60´s by Redman and Steward:[4] hexagonal wurtzite-CoO and cubic zinc blende-CoO. The latter can be found in highly defected rock salt-CoO, as possible defected structures in non-stoichiometric rock-salt crystals[5] or as a by-product in Li-Co oxide batteries.[6,7] Moreover, zinc blende-CoO has been used as seed for the growth of rock salt-CoO and Co multipods[8] and exhibits appealing semiconducting properties.[9] However, very little is known about the magnetism of zinc blende-CoO.[4–12] Although its magnetic properties have not been elucidated experimentally, theoretical studies predict an antiferromagnetic order.[13,14] Concerning wurtzite-CoO, more systematic studies have only recently been carried out. In particular, wurtzite-CoO has been found to be rather stable in nanoparticle form[15–19] and has been reported to have appealing catalytic, optical, semiconducting, electrochemical and biomedical properties,[20–26] with possible applications in lithium batteries,[27] solar energy conversion,[28] photoacoustic imaging[24,27] and water splitting.[29] In addition, this structure has been shown to appear as a strain relief or polarity compensation phase in rock salt-CoO thin films,[28,30–37] as phase separation in Co-doped ZnO ultrathin films[38] and in passivation CoO shells of Co nanoparticles.[39,40] However, it was probably the suggestion that wurtzite-CoO could be the origin of the room temperature ferromagnetism in $Zn_{1-x}Co_xO$ diluted magnetic semiconductors,[41] which triggered a renewed interest in this phase. Despite extensive studies

in nanoparticles and thin films, the magnetic properties of wurtzite-CoO remain rather controversial. From a theoretical point of view, most studies agree that wurtzite-CoO is antiferromagnetic, although different, collinear and non-collinear, structures have been proposed in simulations for pure CoO,[13,42–45], doped wurtzite-CoO[41,46–49] or wurtzite-CoO thin films.[32,50] Additionally, it has been shown that surface effects and bulk defects (e.g., vacancies) may lead to uncompensated spins resulting in a ferromagnetic-like response.[13,41,45,46] Experimentally, opposing magnetic behaviors have been reported for wurtzite-CoO, ranging from antiferromagnetic or ferromagnetic-like to paramagnetic.[24,51–62] This probably stems from the strong magnetic signal of the uncompensated spins which smears out any intrinsic magnetic properties of wurtzite-CoO. The lack of a systematic magnetic characterization sets an obstacle for the full understanding and the development of novel applications in wurtzite-CoO.

To elucidate the magnetic properties of wurtzite-CoO and zinc blende-CoO we developed a *large scale* nanoparticle synthesis that allowed carrying out a rational investigation of their structural and magnetic properties comprising a comprehensive magnetic and powder neutron diffraction study. The results indicate that zinc blende-CoO is antiferromagnetic with a 3rd type structure and a Néel temperature of about T_N (zinc blende) ~ 225 K. On the other hand although wurtzite-CoO exhibits also an antiferromagnetic order (with a rather complex structure) with T_N ~ 110 K, the uncompensated spins overwhelm the magnetization behavior leading to a ferromagnetic-like response.

2. Results and Discussion

The fits of the x-ray diffraction (XRD) patterns determine that the nanoparticles synthesized in a small batch present a pure wurtzite-CoO structure (space group $P6_3mc$) with hexagonal lattice parameters a = 3.2509(3) Å and c = 5.1954(5) Å (where the values in brackets correspond to the estimated standard deviation with a 76% of confidence interval, taking into

account both statistical and systematic errors) and a crystallite size, <D>, of $<D>_W$ = 17(1) nm (**Figure 1**a). The values for a and c are in line with previously reported lattice parameters of wurtzite-CoO (JCPDS no. 80-0075).[4,51,52,54,56,61,63] On the other hand, the sample obtained in a large batch shows a mixture of wurtzite-CoO (a = 3.2526(1) Å, c = 5.1976(1) Å; $<D>_W$ = 32.0(5) nm) and cubic zinc blende-CoO structures (space group $F\bar{4}3m$; a = 4.5533(1) Å, $<D>_{ZB}$ = 13.0(5) nm - **Figure 1**b). The volume ratio of the two phases, wurtzite/zinc blende, is 63/37. Moreover, the fit of the mixed sample (synchrotron data) reveals that both phases present oxygen vacancies and that wurtzite shows also microstrains. Using different concentrations of both oleic acid and cobalt (II) acetylacetonate has been shown to be a good strategy to obtain different CoO polymorphs. The zinc blende polymorph has been reported as the primary phase of the particles once they had nucleated under this synthetic conditions, even this is not the most stable phase, which suggest the reaction is kinetically controlled[12]. Then, wurtzite CoO is formed by nucleation on growth faults or pre-existing boundaries on zinc blende crystals. The final product is strongly related to the zinc blende crystallite size. In the large batch, under high-concentrated precursors conditions, the transformation from zinc blende to wurtzite is only partial because part of the zinc blende nuclei overcomes a critical radius and it cannot be transformed to wurtzite and, consequently, it can be also found in the final product as a metastable phase.[64] On the other hand, for low-concentrated precursor conditions (small batch) the nucleus size of the generated zinc blende CoO was not large enough so a complete transformation to wurtzite CoO can take place.

Importantly, none of the samples show any traces of the most stable CoO phase (i.e., rock salt-CoO) or metallic Co. Note that from this type of synthesis, which is carried out under inert/mild reducing conditions, it is reported that the rock salt-CoO phase is not formed below 320 ºC[12] unless some surfactants, which acts as catalyzers, are added into the reaction such as oleylamine.[65,66] Interestingly, it has been observed that the use of inert gases such argon or

nitrogen as well as the use of carboxylic acids as surfactants is critical for the formation of the target CoO polymorphs.[4]

The transmission electron microscopy (TEM) characterization of the pure wurtzite-CoO sample shows that nanocrystals have a pyramid shape morphology (similar to the one already reported for wurtzite-CoO)[52–54] with length of the edges between 20 and 30 nm (**Figure 2**a). Note, the TEM image indicates that the particles are coated with a carbon layer as a result of the reaction. The lattice fringes in the high resolution-TEM (HR-TEM) images corroborate the interplanar distance of the (002) crystal plane from wurtzite-CoO (**Figure 2**b). Moreover, the selected area electron diffraction (SAED) pattern (**Figure 2**c) confirms the presence of only the wurtzite-CoO phase. In the mixed wurtzite-zinc blende sample, the amount of residual carbonaceous species is much larger than in the pure wurtzite-CoO sample (despite the exhaustive cleaning), which interferes with the imaging of the CoO particles in conventional TEM. However, as can be seen in **Figure S1**, high-angle annular dark-field scanning transmission electron microscopy (HAADF-STEM) imaging (proportional to the atomic number of the ions) enables to unambiguously distinguish the morphology of the samples (compare panels a and b in **Figure S**1). The mixed wurtzite-zinc blende sample (**Figure 2**d,e and **Figure S1**)) displays small aggregates of particles embedded in an amorphous carbon matrix, presenting two distinct types of particles: (i) pyramid-shaped with a length around 30 nm (highlighted by blue triangles in **Figure 2**c and **Figure S1**b, ascribed to the wurtzite-CoO) and (ii) more irregular, spheroidal, particles (highlighted by red circles in **Figure 2**c and **Figure S1**b – corresponding to zinc blende-CoO). Importantly, HAADF-STEM images also confirm that the particles are well-separated from each other by a carbon layer (see yellow arrow in **Figure S1**b). Moreover, the HRTEM images of each type of particle evidence different lattice spacings depending on their shape (**Figure 2**f), where the triangular particles correspond to wurtzite, while the spheroidal particles are zinc blende.

Finally, the SAED analysis corroborates the presence of the two different types of phases in the sample (**Figure 2**g).

The temperature dependence of the magnetization of the pure wurtzite-CoO particles shows a rather featureless behavior down to ~20 K, with a monotonic increase of the magnetization (M) as the temperature decreases (**Figure 3**a). Namely, at first glance there is no obvious sign of any magnetic transition. However, it is important to highlight that the FC and ZFC do not overlap (see **Figure S**2), indicating that the material has a ferromagnetic-like behavior. Analogous results have been previously observed by other authors in wurtzite-CoO.[51–54,56,62] Interestingly, a similar behavior has been also noted in most antiferromagnetic transition-metal oxide nanoparticles (rock salt-CoO, NiO, CuO, MnO). The non-overlapping ZFC-FC curves and lack of any obvious transition is typically ascribed to the presence of uncompensated spins either at the surface (due to surface spin disorder, because of the change in atomic coordination) or in the bulk (due to defects).[67–69] These uncompensated spins have a large magnetization, which overwhelms any signal arising from the antiferromagnet itself, precluding the clear detection of a cusp in M(T) typical of antiferromagnets at their Néel temperature, T_N. A more careful inspection of the ZFC branch of M, evidences a small bump at about 125 K (**Figures 3**c,e,g, right insets). This non-monotonic behavior could tentatively be ascribed to a magnetic transition. Importantly, the cusp is virtually field independent (see **Figure 3**), as expected for a thermodynamic magnetic transition. However, at high fields the signal from the uncompensated spins overwhelms the signal form the magnetic transtion and the cusp is no longer visible (**Figure 3**a). Note that small anomalies in M(T) have been observed in a few cases in wurtzite-CoO, although they were not discussed in detail.[53,56] At very low temperatures a clear transition is observed (**Figure 3**a,c,e,g, left inset) similar to what has been observed by He *et al*. and An *et al.* in wurtzite-CoO[51–53] and in several antiferromagnetic transition metal oxides (e.g., NiO).[70] In concordance with other nanoparticle systems, this transition is ascribed to the slowdown of the thermal fluctuations as

the temperature decreases, followed by the increase of the magnetic correlation of the surface spins that freeze in a spin-glass like state at ~7 K.

The presence of uncompensated spins is confirmed by the hysteresis loop measured at 5 K, which shows a rather large saturation magnetization (M_S) of 25 emu g^{-1}, (i.e., extrapolation of the high field magnetization to H = 0) at low temperatures (**Figure 4**a) and a clear hysteresis. M_S decreases rather fast at low temperatures as the temperature increases, although it levels off at a small, but finite, value above about 100 K; M_S(T > 100 K) = 0.25 emu g^{-1} (**Figure 4**b). Namely, wurtzite-CoO presents a ferromagnetic-like behavior at room temperature. These results are in concordance with earlier studies in wurtzite-CoO, which show a ferromagnetic response,[51–53,62] even at room temperature.[53,62] Note that the strong ferromagnetic-like behavior can be tentatively explained by the presence of uncompensated spins arising from the existence of a rather large amount of oxygen vacancies (note $CoO_{0.7}$ stoichiometry of the particles), with the FM signal being roughly proportional to the number of such vacancies.[71,72] Concerning the dependence of the coercivity, H_C, with temperature it can be observed that at low temperatures, there is an increase in H_C, determined by the increase of the magnetic anisotropy related with the freezing of the surface disorder. However, at higher temperatures, the H_C(T) shows a somewhat unusual behavior, exhibiting a broad maximum at around 100 K (**Figure 4c**). Similar effects have been observed in NiO[67,68] and rock salt CuO[73] and they have been tentatively ascribed to the ordering of the antiferromagnetic core or to a blocked state of the magnetization of the core.[74] In fact, this maximum could be linked to the enhanced coercivity typically observed in ferromagnetic/antiferromagnetic systems at the Néel (or blocking temperature) temperature of the antiferromagnetic counterpart.[75,76] In this framework, and taking into account the bump at about 125 K in M(T), the maximum in H_C could indicate a coupling between the uncompensated spins and an antiferromagnetic phase, hence preliminarily implying an antiferromagnetic character of wurtzite-CoO.

The mixed wurtzite-zinc blende sample exhibits a similar magnetic behavior. The temperature dependence of the magnetization is rather featureless with a peak at very low temperatures (**Figure 3**b). However, careful inspection of the ZFC M(T) evidences that in this case there is small maximum at 225 K (**Figures 3**f,h, right inset), although no clear feature is observed around 100 K (probably concealed by the high slope of M(T) at this temperature range for this sample). The feature in M(T) at 225 K may indicate a second magnetic transition, which in this case could be attributed to zinc blende-CoO. Interestingly, the H_C(T) of the mixed sample apart from the broad maximum at around 100 K (similar to the one observed in the pure wurtzite-CoO), shows a kink at about 225 K (**Figure 4**e). This could corroborate the presence of a second magnetic transition at higher temperatures for the mixed sample ascribed to the antiferromagnetic ordering of the zinc blende-CoO counterpart, with T_N ~ 225 K.

Figure 5a shows the first derivative of the absorption curve measured at $\omega/2\pi$ ~ 24.3 GHz for the pure wurtzite-CoO nanoparticle sample. At room temperature the signal presents a single and nearly symmetric resonance line, centered at the resonance field H_R ~ 7.76 kOe (**Figure 5**a). This H_R corresponds to a g-value of 2.23 which is in agreement with the experimentally observed for Co^{2+}, S = 3/2, which lies in the 2.1-2.8 range.[77–79] When the temperature decreases the asymmetry of the resonance becomes more evident (**Figure 5**a), i.e., a secondary peak splits from the main resonance line and shifts to lower field as the system cools. Note that usually the FMR signal of a powder sample is asymmetric because the material has an angular distribution of the magnetization easy axes respect to the external field. In fact, the observed spectra present a typical FMR line shape with uniaxial anisotropy. Moreover, the anisotropy field $H_A = 2K/M$, which is proportional to the peak-to-peak linewidth, increases when the temperature decreases and at T ~ 110 K the resonance signal vanishes. In order to obtain the physical parameters that characterize the spectra, the lines were fitted using the Smith-Beljers formalism for the case of material with a ferromagnetic component and uniaxial anistotropy.[80,81] Then, from the magnetic free energy of the system

$F=-\boldsymbol{M_S}.\boldsymbol{H}+K\ sin^2\phi$, where K corresponds to the uniaxial effective magnetic anisotropy constant, $\boldsymbol{M_S}$ is the saturation magnetization of the system and ϕ is the angle between the $\boldsymbol{M}$ and the uniaxial axis, the resonance condition is:[82]

$$\left(\frac{\omega}{\gamma}\right)^2 = \left(H\cos(\phi-\phi_H)+H_A\cos^2\phi\right)\left(H\cos(\phi-\phi_H)+H_A\cos 2\phi\right) \qquad (1)$$

where $H_A = 2K/M$ is the anisotropy field, γ is the gyromagnetic ratio, ϕ_H is the angle between H and the uniaxial axis. The resonance field is obtained by solving the Eq. (1) in a self-consistent way for the equilibrium position of the magnetization. Since the sample consists of an ensemble of nanoparticles, we assume that the absorption line corresponds to the sum of resonances, with Lorentzian lineshape, with a homogeneous angular distribution of anisotropy axes in relation to the magnetic field. From the fits of the FMR resonances at each temperature (**Figure 5**a) the adjusted parameters: H_R, H_A and the FMR intensity, I_{FMR}, were obtained (**Figure 5**b). Note that H_A increases from 0.5 kOe at room temperature to 3.30 kOe at T = 130 K as the temperature decreases. This behavior originates from the temperature dependence of the different contributions to the effective anisotropy, as the magnetocrystalline anisotropy[83–85] and the demagnetizing field, which increases as the temperature decreases. Moreover, due to the thermal fluctuations of the magnetic moment, in nanoparticles the effective anisotropy tends to decrease as the temperature increases.[82,86,87] Interestingly, at low temperatures, H_R shifts with respect to the expected one from the Co^{2+} g-value. This behavior has been observed in several FMR studies of nanoparticles and it is ascribed to the presence of additional internal fields, usually produced by dipolar or exchange interparticle interactions, which shift the resonance toward lower fields.[82,87,88] **Figure 5**b shows also a remarkable decrease of H_R and I_{FMR} below ~130 K, followed by the disappearance of the signal at T ~ 110 K. This behavior is typically found when the system develops an antiferromagnetic transition, where the antiferromagnetic resonance mode can no longer be excited due to the presence of large anisotropies and exchange fields.[89] Note that

the antiferromagnetic transition is usually smoother in nanoparticles[85] than in bulk materials.[90] Remarkably, the loss of I_{FMR} below T_N indicates that the uncompensated spins must be strongly coupled, leading to an increased magnetic anisotropy. As a consequence, when the nanoparticle orders antiferromagnetically, the signal of the uncompensated spins is also lost, because the resonance frequency is larger than the excitation microwave frequency.[85] This fact makes it impossible to study the features related to the coupling between the uncompensated and antiferromagnetic spins using FMR (as it is often done in weakly coupled ferro(i)magnetic/antiferromagnetic thin film and core/shell systems[76,91–93]). Similarly, the vanishing I_{FRM} also prevents observing any features related to the spin glass-like transition observed in the M(T) data.[94,95]

Similar to the pure wurtzite-CoO nanoparticles, the mixed sample shows at room temperature a single resonance line centered at H_R ~ 7.60 kOe, which corresponds to a g-value of ~2.27. The inhomogeneously broadened line observed in the whole temperature range probably stems from the convolution of several resonances. In fact, the resonance in the mixed sample is considerably broader than in pure sample, which does not allow an easy deconvolution and, consequently, it precludes obtaining information on the internal structure. For example, while the peak-to-peak linewidth at room temperature is ΔH_{pp} ~ 1.8 kOe for pure wurtzite-CoO, it becomes ΔH_{pp} ~ 4.0 kOe for the mixed sample. The H_R, ΔH and I_{FMR} resonance parameters where obtained by fitting the experimental spectra to a Lorentzian lineshape curve (**Figure 5**c). In contrast to the pure wurtzite sample, the FMR parameters exhibit a rather smooth evolution with temperature down to low temperatures (**Figure 5**d). However, a change in slope is observed for H_R, ΔH and I_{FMR} around 240 K and 110 K. Since these temperatures are close to the transition temperatures of zinc blende (~225 K) and wurtzite (~110 K) CoO structure hinted in the magnetic measurements, these features can be associated with the successive magnetic ordering of the different CoO phases. Therefore, below T ~ 240 K the

ΔH and I_{FMR} increase as a consequence of the FMR of the uncompensated moment of the zinc blende magnetic phase, which probably shows a resonance line down to low temperatures. Besides, at T ~ 110 K the wurtzite-CoO phase orders antiferromagnetically and it no longer contributes to the resonance, as a consequence the ΔH and I_{FMR} slope decrease.

To confirm the presence of uncompensated spins we carried out XMCD measurements. As can be seen in **Figure 6**, the XMCD measurements at 15 K of both the pure and mixed samples show a clear ferromagnetic signal. Interestingly, there is no sign of metallic Co neither in the XAS (not shown) nor in the XMCD, indicating the magnetic signal arises from the oxides. In fact, simulations of the XMCD results indicate that the signal arises predominantly from Co^{2+} ions in tetrahedral positions, as expected for wurtzite and zinc blende-CoO (see Supplementary Information, Figure S3).[96–98] Moreover, the XMCD signal at 300 K is considerable weaker than at low temperatures, where the magnetic moment (roughly proportional to the area of the XMCD spectra) decreases a factor 100 from 15 K to 300 K (**Figure 6**, inset), in full agreement with the temperature dependence of M_S, hence, corroborating the uncompensated spins as the origin of the ferromagnetic-like behavior in the samples. The uncompensated spins probably arise from surface effects and due to internal defects such as oxygen vacancies or stacking faults.

To be able to unambiguously determine the nature of the magnetic phases we carried out neutron diffraction experiments. However, the amount of sample synthesized in a small batch, the organic material present in the sample (surfactants) and the nanocrystalline character of the sample, led to exceedingly noisy neutron diffraction patterns to perform any quantitative analysis. Thus, the experiment was carried out only in the mixed wurtzite zinc blende-CoO sample (obtained from the large batch). The low temperature patterns clearly show the presence of magnetic peaks in both the zinc blende and the wurtzite structures (**Figure 7**a). This is in contrast to the only existing neutron diffraction study on wurtzite CoO, in which only a small broad magnetic peak at low temperatures was observed and ascribed to a

frustrated short range magnetic order.[56] It is worth emphasizing the magnetic peaks in the neutron diffraction pattern correspond only to either zinc blende or wurtzite CoO, consequently, discarding any other ordered magnetic phases in the sample.

The fitting of the neutron diffraction pattern shows that the zinc blende-CoO structure presents a simple antiferromagnetic order with a magnetic structure of the 3rd type in a face centred cubic lattice (following Corliss-Elliot-Hasting notation)[99] with an average magnetic moment of 2.3(3) μ_B/ion. This structure is similar to the zinc blende structure of α-MnS, with the magnetic moments ordered along the x-axis and consist in a spin configuration where 2/3 of the neighbors spins are antiparallel and 1/3 parallel per each Co^{2+} ion. For the next-nearest neighbors 1/3 of the spins are aligned antiparallel and 2/3 parallel.[99] The experimentally obtained magnetic moment is in concordance with theoretical predictions of zinc blende-CoO, 2.74 μ_B/ion.[13] The temperature dependence of the magnetic peaks of the zinc blende-CoO shows that this phase remains clearly magnetic up to 110 K (**Figure 7**b). However, room temperature measurements evidence that 300 K is already above its T_N. A fit of the temperature dependence of the intensity of the main magnetic peak to a mean field dependence of the magnetic moment, $\mu \alpha (T-T_N)^{1/2}$, renders approximately $T_N \sim 205$ K. This value is in rough agreement with the T_N values inferred from the other magnetic characterizations ($T_N \sim 225$ K), taking into account the simplicity of the fit.

On the other hand, the magnetic structure of the wurtzite-CoO phase is much more complex. Namely, the magnetic moments are tilted due to the coexistence of two different magnetic orders within the structure. Along the c-axis the Co atoms are ordered antiferromagnetically, with a 2nd type structure (following Corliss-Elliot-Hasting notation,[99] similar to the β-MnS wurtzite structure[99]) and a magnetic moment of 1.4(1) μ_B/ion. In the 2nd type antiferromagnetic structure half of the nearest neighbors are aligned antiparallel and the other half parallel. In addition, all the next-nearest neighbors are aligned antiparallel.[99]

Additionally, in the plane, the atoms present a rather unusual incommensurate magnetic order along the y-axis with 2.8(2) μ_B/ion. That is, the magnetic periodicity does not correspond with the structural order.[100,101] Instead of the expected Néel type order with a wave vector of k = 0, ½, 0, it shows k = 0, 0.4559(3), 0. The combination between the commensurate order along the c-axis and the incommensurate structure in the y-axis implies that each atom has a different tilt angle, ranging from 0° (spins along the c-axis) to 63°. Moreover, this incommensurate structure presents only a short-range order, since it has a small correlation length along the c-axis. Remarkably, the temperature dependence of both magnetic structures shows a T_N ~ 109 K (**Figure 7**b). This T_N is consistent with the transition temperatures inferred from the other techniques.

The origin of this complex magnetic structure in wurtzite-CoO may arise from the arrangement of the Co-O-Co atoms in the hexagonal structure which should weaken and geometrically frustrate the super-exchange between the Co atoms (since there is no way to arrange the spins to satisfy all the interactions simultaneously),[44,59] in contrast to the Co-O-Co alignment in the cubic rock salt-CoO that favors conventional antiferromagnetic arrangements.[102] In fact, the frustration of the wurtzite structure may be the origin of the diversity in the reported magnetic results in wurtzite-CoO, where defects not only induce uncompensated spins,[103] but they may also stabilize the antiferromagnetic order by lifting the degeneracy inherent in frustrated spin arrangements (as for example observed in pyrochlore, kagomé or some spinel structures),[104,105] leading to a long range magnetic order. Hence, depending on the morphology or size of the wurtzite-CoO specimen or the amount and type of defects in its structure (e.g., oxygen vacancies, stacking faults and so on; which are given by the synthetic conditions), dissimilar magnetic behaviors may manifest.

The antiferromagnetic order obtained for both wurtzite-CoO and zinc blende-CoO is consistent with the theoretical predictions,[13,32,41–50] although for wurtzite-CoO the magnetic order is far more complex than theoretically proposed. Interestingly, the results on wurtzite-

CoO are also consistent with single crystalline wurtzite $Zn_{1-x}Co_xO$ films with large Co contents (x = 0.6), which show an antiferromagnetic order with uncompensated spins.[96,97]

3. Conclusions

Summarizing, a systematic study of the magnetic properties of the wurtzite and zinc blende nanoscale polymorphs of CoO has been performed. Notably, the results evidence that although the intrinsic magnetic order of both wurtzite and zinc blende-CoO is antiferromagnetic, the systems present a large number of uncompensated spins which result in a ferromagnetic-like behavior even at room temperature. Moreover, while zinc blende-CoO shows a rather simple spin structure, the one for wurtzite-CoO is somewhat complex, comprising two different magnetic components (one of them incommensurate) orthogonal to each other.

4. Experimental Section

The synthesis of CoO nanoparticles has been carried out by thermal decomposition of cobalt (II) acetylacetonate ($Co(acac)_2$) in the presence of oleic acid and 1-octadecene. Two different reactions were carried out: (i) *small batch*: 1 g $Co(acac)_2$ (~ 4 mmol, Aldrich 97%) and 0.5 g oleic acid (1.8 mmol, Alfa Aesar 90%) were mixed with 20 mL 1-octadecene (97%, Acros Organics) –this type of synthesis typically renders about 100-150 mg of sample–; (ii) *large batch*: 5 g $Co(acac)_2$ (20 mmol) were mixed with 2.5 g oleic acid (9 mmol) with 20 mL 1-octadecene (this approach leads to 1.45 g of sample). Both types of mixtures were degassed at room temperature and then heated up to 300 ºC at a heating rate of 3 $ºC \cdot min^{-1}$ under argon flow, keeping the reflux for 30 minutes. Finally, the slurries were cooled down to room temperature and CoO nanoparticles were washed with toluene and 2-propanol and the powder was collected by centrifugation and dried with nitrogen flow.

Powder x-ray diffraction (XRD) was performed at the BL04-MSPD beamline at the ALBA Synchrotron (Barcelona, Spain), with a wavelength of 0.4131 Å and with a Panalytical X'Pert Pro diffractometer with Cu K_α radiation (1.5418 Å). Note that the synchrotron powder diffraction patterns show that any impurity phases must be less than 1-2%.

The morphology of nanoparticles was characterized by transmission electron microscopy, using a FEI Tecnai G2 F20 HR(S)TEM microscope operated at 200 kV, equipped with selected area electron diffraction, SAED. High-angle annular dark-field scanning transmission electron microscopy (HAADF-STEM) and high resolution transmission electron microscopy (HR-TEM) images were also acquired using the same microscope. The CoO nanoparticles were deposited on lacey carbon Cu TEM grids from a very diluted hexane suspension after strong sonication for 5 min. The TEM grids were heated at 120 ºC for 12 hours under ultrahigh vacuum to reduce organic residue formed as by-product during CoO nanoparticle synthesis. Finally, the grids were subjected to an argon plasma treatment for 2 min prior to imaging to further reduce the carbonaceous remains.

Moreover, the chemical composition of the samples was determined by energy dispersive x-ray spectroscopy (EDX) using a EDS/EDX Oxford LINCA detector attached to a 200 keV JEOL JEM-2011 microscope. The acquisition time was set to 90 s. The EDX analyses (Figure S4) confirm that no magnetic ions (e.g., Fe, Ni or Mn) apart from Co are present in any of the samples. Note that for EDX characterization, to reduce the high content in carbon arising from the surfactants and the byproducts, the CoO nanoparticles were transfered to ethanol by ligand exchange with dimercaptosuccinic acid to remove the oleic acid from the particle surface and part of the carbon generated during the reaction.

Magnetization measurements were carried out using a superconducting quantum design magnetometer (MPMS, Quantum Design) and a vibrating sample magnetometer (PPMS, Quantum Design). The measurements of the temperature dependence of magnetization, M(T), were carried out at 100 Oe after either zero field cooling (ZFC) or field cooling (FC) in 25,

100, 1000 or 10000 Oe from 320 K to 5 K. Hysteresis loops, M(H), with a maximum applied field of 50 kOe, were obtained after ZFC from 320 to 5 K. The loops were obtained sequentially at increasing fixed temperatures.

Ferromagnetic resonance (FMR) measurements were taken with a commercial Bruker ESP300 spectrometer at a frequency of ν = 24.3 GHz (K-band) in the 6 – 300 K temperature range. The spectra were recorded as the first derivative of the FMR absorption curve. Note that magnetic resonance is a very sensitive technique to detect paramagnetic or ferromagnetic impurities. Although at high temperature any impurity signal could be hidden by the resonance of the wurtzite or zinc blende CoO majority phases, possible impurities should be detected below 100 K in the pure wurtzite sample, since the signal of the wurtzite phase vanishes due to the antiferromagnetic order. The absence of any lines at low temperature allows excluding the presence of any magnetic spurious phases.

X-ray absorption spectroscopy (XAS) and x-ray magnetic circular dichroism (XMCD) experiments were carried out at BL29 (BOREAS) beamline of the ALBA synchrotron (Barcelona, Spain). The spectra were recorded at the Co $L_{2,3}$ edges using total electron yield mode at 10 K in a 50 kOe magnetic field. The simulation of the XMCD spectra were carried out using the CTM4XAS Program.[106]

Powder neutron diffraction was carried out at the D1B beamline in the Institute Laue Langevin (ILL; Grenoble, France), with a neutron wavelength of 2.524 Å. All diffraction patterns (XRD and neutrons) were analyzed using FullProf.[107]

Supporting Information

Supporting Information is available from the Wiley Online Library or from the author.

Acknowledgements

This work was supported by the 2014-SGR-1015 project of the Generalitat de Catalunya. EW and RDZ thank ANPCyT and CONICET Argentine for support through Grants No. PICT-2015-0883 and PIP 112-20110100519, respectively. I.V.G. acknowledges the support of the

Russian grants RFBR 16-02-00058 and RG 14.B25.31.0025. We also acknowledge the ALBA Synchrotron Light Facility for the provision of synchrotron beamtime and the Institute Laue-Langevin (ILL) and the Spanish Initiatives on Neutron Scattering (SpINS) for the provision of neutron beamtime. AGR thanks the Beatriu de Pinos Fellowship (ref 2011 BP_B 00209) and ALO acknowledges the Juan de la Cierva Program (MINECO IJCI-2014-21530). ICN2 is funded by the CERCA Programme/Generalitat de Catalunya. ICN2 also acknowledges the support from the Severo Ochoa Program (MINECO, grant SEV-2013-0295).

References

[1] C. R. A. Catlow, A. N. Cormack, F. Théobald, *Acta Crystallogr. Sect. B Struct. Sci.* **1984**, *40*, 195.

[2] C. Ma, A. Navrotsky, *Chem. Mater.* **2012**, *24*, 2311.

[3] T.-H. Lee, Y.-X. Yao, V. Stevanović, V. Dobrosavljević, N. Lanatà, *http://arxiv.org/abs/1710.08586*

[4] M. J. Redman, E. G. Steward, *Nature* **1962**, *193*, 867.

[5] R. W. Grimes, A. B. Anderson, A. H. Heuer, *J. Am. Ceram. Soc.* **1986**, *69*, 619.

[6] M. N. Obrovac, J. R. Dahn, *Electrochem. Solid-State Lett.* **2002**, *5*, A70.

[7] M. N. Obrovac, R. A. Dunlap, R. J. Sanderson, J. R. Dahn, *J. Electrochem. Soc.* **2001**, *148*, A576.

[8] Y. C. Sui, Y. Zhao, J. Zhang, S. Jaswal, X. Z. Li, D. J. Sellmyer, *IEEE Trans. Magn.* **2007**, *43*, 3115.

[9] S. Lany, *J. Phys. Condens. Matter* **2015**, *27*, 283203.

[10] J. DiCarlo, A. Navrotsky, *J. Am. Ceram. Soc.* **1993**, *76*, 2465.

[11] R. W. Grimes, A. N. Fitch, *J. Mater. Chem.* **1991**, *1*, 461.

[12] R. W. Grimes, K. P. D. Lagerlof, *J. Am. Ceram. Soc.* **1991**, *74*, 270.

[13] T. Archer, R. Hanafin, S. Sanvito, *Phys. Rev. B* **2008**, *78*, 014431.

[14] A. Zayed, A. M. Márquez, J. F. Sanz, *J. Phys. Chem. C* **2013**, *117*, 22714.

[15] V. Papaefthimiou, T. Dintzer, V. Dupuis, A. Tamion, F. Tournus, D. Teschner, M.

Hävecker, A. Knop-Gericke, R. Schlögl, S. Zafeiratos, *J. Phys. Chem. Lett.* **2011**, *2*, 900.

[16] B. Yang, G. Khadra, J. Tuaillon-Combes, E. C. Tyo, M. J. Pellin, B. Reinhart, S. Seifert, X. Chen, V. Dupuis, S. Vajda, *J. Phys. Chem. C* **2016**, *120*, 21496.

[17] V. Papaefthimiou, T. Dintzer, V. Dupuis, A. Tamion, F. Tournus, A. Hillion, D. Teschner, M. Hävecker, A. Knop-Gericke, R. Schlögl, S. Zafeiratos, *ACS Nano* **2011**, *5*, 2182.

[18] J. H. Shim, K. M. Nam, W. S. Seo, H. Song, J. T. Park, *Chem. - An Asian J.* **2011**, *6*, 1575.

[19] M. Jae Kwon, H. Jung, J. Hoon Park, *J. Phys. Chem. Solids* **2012**, *73*, 1448.

[20] K. M. Nam, J. H. Shim, D.-W. Han, H. S. Kwon, Y.-M. Kang, Y. Li, H. Song, W. S. Seo, J. T. Park, *Chem. Mater.* **2010**, *22*, 4446.

[21] J.-M. Wu, L.-J. Chen, X.-B. Yang, Y.-J. Zhao, *Phys. Lett. A* **2014**, *378*, 2635.

[22] A. Lu, Y. Chen, D. Zeng, M. Li, Q. Xie, X. Zhang, D.-L. Peng, *Nanotechnology* **2014**, *25*, 035707.

[23] A. V. Ravindra, B. C. Behera, P. Padhan, *J. Nanosci. Nanotechnol.* **2014**, *14*, 5591.

[24] Y. Kimura, T. Kurimoto, Y. Imai, H. Sugii, A. Toshimitsu, T. Matsuda, H. Imai, H. Yamada, T. Kondo, *JSM Biotechnol Bioeng* **2014**, *2*, 1043.

[25] G. Velegraki, J. Miao, C. Drivas, B. Liu, S. Kennou, G. S. Armatas, *Appl. Catal. B Environ.* **2018**, *221*, 635.

[26] C. Guo, Y. Zheng, J. Ran, F. Xie, M. Jaroniec, S.-Z. Qiao, *Angew. Chemie Int. Ed.* **2017**, *56*, 8539.

[27] K. M. Nam, Y. C. Choi, S. C. Jung, Y.-I. Kim, M. R. Jo, S. H. Park, Y.-M. Kang, Y.-K. Han, J. T. Park, *Nanoscale* **2012**, *4*, 473.

[28] S. Mohr, T. Schmitt, T. Döpper, F. Xiang, M. Schwarz, A. Görling, M. A. Schneider, J. Libuda, *Langmuir* **2017**, *33*, 4178.

[29] K. Y. Jang, G. Park, K. H. Oh, J. H. Seo, K. M. Nam, *Chem. Commun.* **2017**, *53*, 4120.

[30] W. Meyer, D. Hock, K. Biedermann, M. Gubo, S. Müller, L. Hammer, K. Heinz, *Phys. Rev. Lett.* **2008**, *101*, 016103.

[31] K. Heinz, L. Hammer, *J. Phys. Condens. Matter* **2013**, *25*, 173001.

[32] A. S. Walton, J. Fester, M. Bajdich, M. A. Arman, J. Osiecki, J. Knudsen, A. Vojvodic, J. V. Lauritsen, *ACS Nano* **2015**, *9*, 2445.

[33] D. Eom, *J. Korean Phys. Soc.* **2015**, *67*, 1792.

[34] T. Xu, M. Schwarz, K. Werner, S. Mohr, M. Amende, J. Libuda, *Chem. - A Eur. J.* **2016**, *22*, 5384.

[35] J. Fester, M. Bajdich, A. S. Walton, Z. Sun, P. N. Plessow, A. Vojvodic, J. V. Lauritsen, *Top. Catal.* **2017**, *60*, 503.

[36] J. Fester, A. Walton, Z. Li, J. V. Lauritsen, *Phys. Chem. Chem. Phys.* **2017**, *19*, 2425.

[37] J. Fester, M. García-Melchor, A. S. Walton, M. Bajdich, Z. Li, L. Lammich, A. Vojvodic, J. V. Lauritsen, *Nat. Commun.* **2017**, *8*, 14169.

[38] H. L. Meyerheim, C. Tusche, A. Ernst, S. Ostanin, I. V. Maznichenko, K. Mohseni, N. Jedrecy, J. Zegenhagen, J. Roy, I. Mertig, J. Kirschner, *Phys. Rev. Lett.* **2009**, *102*, 156102.

[39] T.-J. Kühn, W. Caliebe, N. Matoussevitch, H. Bönnemann, J. Hormes, *Appl. Organomet. Chem.* **2011**, *25*, 577.

[40] T.-J. Kühn, J. Hormes, N. Matoussevitch, H. Bönnemann, P. Glatzel, *Inorg. Chem.* **2014**, *53*, 8367.

[41] T. Dietl, T. Andrearczyk, A. Lipińska, M. Kiecana, M. Tay, Y. Wu, *Phys. Rev. B* **2007**, *76*, 155312.

[42] M. J. Han, H.-S. Kim, D. G. Kim, J. Yu, *Phys. Rev. B* **2013**, *87*, 184432.

[43] M. Han, J. Yu, *J. Korean Phys. Soc.* **2006**, *48*, 1496.

[44] R. Hanafin, T. Archer, S. Sanvito, *Phys. Rev. B* **2010**, *81*, 054441.

[45] M. Y. Yin, X. C. Wang, W. B. Mi, G. F. Chen, B. H. Yang, *J. Alloys Compd.* **2014**, *610*, 422.

[46] M. Y. Yin, X. C. Wang, W. B. Mi, Y. H. Ding, G. F. Chen, B. H. Yang, *Comput. Mater. Sci.* **2014**, *93*, 193.

[47] R. X. Liu, X. C. Wang, G. F. Chen, B. H. Yang, *Phys. E (Amsterdam, Neth.)* **2015**, *74*, 226.

[48] S. K. Nayak, M. Ogura, A. Hucht, H. Akai, P. Entel, *J. Phys. Condens. Matter* **2009**, *21*, 064238.

[49] R. X. Liu, X. C. Wang, G. F. Chen, B. H. Yang, *Phys. E (Amsterdam, Neth.)* **2016**, *77*, 149.

[50] S. Roy, H. L. Meyerheim, K. Mohseni, Z. Tian, D. Sander, M. Hoffmann, W. Adeagbo, A. Ernst, W. Hergert, R. Felici, J. Kirschner, *Phys. Rev. B* **2014**, *89*, 165428.

[51] X. He, W. Zhong, S. Yan, C. Liu, H. Shi, C.-T. Au, Y. Du, *J. Phys. Chem. C* **2014**, *118*, 13898.

[52] X. He, H. Shi, *Mater. Res. Bull.* **2011**, *46*, 1692.

[53] K. An, N. Lee, J. Park, S. C. Kim, Y. Hwang, J.-G. Park, J.-Y. Kim, J.-H. Park, M. J. Han, J. Yu, T. Hyeon, *J. Am. Chem. Soc.* **2006**, *128*, 9753.

[54] W. S. Seo, J. H. Shim, S. J. Oh, E. K. Lee, N. H. Hur, J. T. Park, *J. Am. Chem. Soc.* **2005**, *127*, 6188.

[55] X. Deng, D. Yang, G. Tan, X. Li, J. Zhang, Q. Liu, H. Zhang, N. J. Mellors, D. Xue, Y. Peng, *Nanoscale* **2014**, *6*, 13710.

[56] A. S. Risbud, L. P. Snedeker, M. M. Elcombe, A. K. Cheetham, R. Seshadri, *Chem. Mater.* **2005**, *17*, 834.

[57] A. V. Ravindra, B. C. Behera, P. Padhan, O. I. Lebedev, W. Prellier, *J. Appl. Phys.* **2014**, *116*, 033912.

[58] M. A. White, S. T. Ochsenbein, D. R. Gamelin, *Chem. Mater.* **2008**, *20*, 7107.

[59] J. Alaria, N. Cheval, K. Rode, M. Venkatesan, J. M. D. Coey, *J. Phys. D. Appl. Phys.* **2008**, *41*, 135004.

[60] X. M. He, W. Zhong, Y. W. Du, *J. Appl. Phys.* **2015**, *117*, 043905.

[61] X. He, X. Song, W. Qiao, Z. Li, X. Zhang, S. Yan, W. Zhong, Y. Du, *J. Phys. Chem. C* **2015**, *119*, 9550.

[62] Q. Qi, Y. Chen, L. Wang, D. Zeng, D.-L. Peng, *Nanotechnology* **2016**, *27*, 455602.

[63] J. F. Liu, S. Yin, H. P. Wu, Y. W. Zeng, X. R. Hu, Y. W. Wang, G. L. Lv, J. Z. Jiang, *J. Phys. Chem. B* **2006**, *110*, 021588.

[64] F. Huang, J. F. Banfield, *J. Am. Chem. Soc.* **2005**, *127*, 4523.

[65] H.-T. Zhang, X.-H. Chen, *Nanotechnology* **2005**, *16*, 2288.

[66] K. M. Nam, W. S. Seo, H. Song, J. T. Park, *NPG Asia Mater.* **2017**, *9*, e364.

[67] E. Winkler, R. D. Zysler, M. V. Mansilla, D. Fiorani, *Phys. Rev. B* **2005**, *72*, 132409.

[68] N. Rinaldi-Montes, P. Gorria, D. Martínez-Blanco, A. B. Fuertes, L. F. Barquín, I. Puente-Orench, J. A. Blanco, *Nanotechnology* **2015**, *26*, 305705.

[69] N. Fontaíña-Troitiño, S. Liébana-Viñas, B. Rodríguez-González, Z.-A. Li, M. Spasova, M. Farle, V. Salgueiriño, *Nano Lett.* **2014**, *14*, 640.

[70] N. Rinaldi-Montes, P. Gorria, D. Martínez-Blanco, A. B. Fuertes, L. Fernández Barquín, J. Rodríguez Fernández, I. de Pedro, M. L. Fdez-Gubieda, J. Alonso, L. Olivi, G. Aquilanti, J. A. Blanco, *Nanoscale* **2014**, *6*, 457.

[71] G. Yang, D. Gao, Z. Shi, Z. Zhang, J. Zhang, J. Zhang, D. Xue, *J. Phys. Chem. C* **2010**, *114*, 21989.

[72] D. P. Dutta, G. Sharma, P. K. Manna, A. K. Tyagi, S. M. Yusuf, *Nanotechnology* **2008**, *19*, 245609.

[73] A. Punnoose, H. Magnone, M. S. Seehra, J. Bonevich, *Phys. Rev. B* **2001**, *64*, 174420.

[74] E. Winkler, R. D. Zysler, M. Vasquez Mansilla, D. Fiorani, D. Rinaldi, M. Vasilakaki, K. N. Trohidou, *Nanotechnology* **2008**, *19*, 185702.

[75] J. Nogués, J. Sort, V. Langlais, V. Skumryev, S. Suriñach, J. S. Muñoz, M. D. Baró, *Phys. Rep.* **2005**, *422*, 65.

[76] M. Estrader, A. López-Ortega, I. V. Golosovsky, S. Estradé, A. G. Roca, G. Salazar-Alvarez, L. López-Conesa, D. Tobia, E. Winkler, J. D. Ardisson, W. A. A. Macedo, A. Morphis, M. Vasilakaki, K. N. Trohidou, A. Gukasov, I. Mirebeau, O. L. Makarova, R. D. Zysler, F. Peiró, M. D. Baró, L. Bergström, J. Nogués, *Nanoscale* **2015**, *7*, 3002.

[77] M. T. Werth, S.-F. Tang, G. Formicka, M. Zeppezauer, M. K. Johnson, *Inorg. Chem.* **1995**, *34*, 218.

[78] N. I. Neuman, E. Winkler, O. Peña, M. C. G. Passeggi, A. C. Rizzi, C. D. Brondino, *Inorg. Chem.* **2014**, *53*, 2535.

[79] P. Sati, R. Hayn, R. Kuzian, S. Régnier, S. Schäfer, A. Stepanov, C. Morhain, C. Deparis, M. Laügt, M. Goiran, Z. Golacki, *Phys. Rev. Lett.* **2006**, *96*, 017203.

[80] J. Smith, H. Beljers, *Phillips Res. Rep* **1955**, *10*, 113.

[81] C. Vittoria, *Microwave Properties of Magnetic Films*, World Scientific, **1993**.

[82] E. de Biasi, C. A. Ramos, R. D. Zysler, *J. Magn. Magn. Mater.* **2003**, *262*, 235.

[83] C. Zener, *Phys. Rev.* **1954**, *96*, 1335.

[84] K. Dwight, N. Menyuk, *Phys. Rev.* **1960**, *119*, 1470.

[85] D. Tobia, E. Winkler, R. D. Zysler, M. Granada, H. E. Troiani, *Phys. Rev. B* **2008**, *78*, 104412.

[86] R. S. de Biasi, T. C. Devezas, *J. Appl. Phys.* **1978**, *49*, 2466.

[87] F. Gazeau, J. Bacri, F. Gendron, R. Perzynski, Y. Raikher, V. Stepanov, E. Dubois, *J. Magn. Magn. Mater.* **1998**, *186*, 175.

[88] C. G. Verdes, B. Ruiz-Diaz, S. M. Thompson, R. W. Chantrell, A. Stancu, *J. Appl. Phys.* **2001**, *89*, 7475.

[89] A. H. Morris, *The Physical Principles of Magnetism*, Wiley-IEEE Press, **2001**.

[90] M. T. Causa, E. Winkler, D. Tobía, M. Tovar, *Phys. B (Amsterdam, Neth.)* **2007**, *398*,

464.

[91] F. Zighem, Y. Roussigné, S.-M. Chérif, P. Moch, J. Ben Youssef, F. Paumier, *J. Phys. Condens. Matter* **2010**, *22*, 406001.

[92] C. Leighton, H. Suhl, M. J. Pechan, R. Compton, J. Nogués, I. K. Schuller, *J. Appl. Phys.* **2002**, *92*, 1483.

[93] A. C. Gandhi, J. G. Lin, *J. Phys. Condens. Matter* **2017**, *29*, 215802.

[94] E. Winkler, R. D. Zysler, D. Fiorani, *Phys. Rev. B* **2004**, *70*, 174406.

[95] D. Tobia, E. L. Winkler, R. D. Zysler, M. Granada, H. E. Troiani, *J. Alloys Compd.* **2010**, *495*, 520.

[96] V. Ney, B. Henne, J. Lumetzberger, F. Wilhelm, K. Ollefs, A. Rogalev, A. Kovacs, M. Kieschnick, A. Ney, *Phys. Rev. B* **2016**, *94*, 224405.

[97] B. Henne, V. Ney, K. Ollefs, F. Wilhelm, A. Rogalev, A. Ney, *Sci. Rep.* **2015**, *5*, 16863.

[98] M. Kobayashi, Y. Ishida, J. l. Hwang, T. Mizokawa, A. Fujimori, K. Mamiya, J. Okamoto, Y. Takeda, T. Okane, Y. Saitoh, Y. Muramatsu, A. Tanaka, H. Saeki, H. Tabata, T. Kawai, *Phys. Rev. B* **2005**, *72*, 201201.

[99] L. Corliss, N. Elliott, J. Hastings, *Phys. Rev.* **1956**, *104*, 924.

[100] M. Gich, C. Frontera, A. Roig, E. Taboada, E. Molins, H. R. Rechenberg, J. D. Ardisson, W. A. A. Macedo, C. Ritter, V. Hardy, J. Sort, V. Skumryev, J. Nogués, *Chem. Mater.* **2006**, *18*, 3889.

[101] D. Kumar, J. K. Galivarapu, A. Banerjee, K. S. Nemkovski, Y. Su, C. Rath, *Nanotechnology* **2016**, *27*, 175702.

[102] J. B. Goodenough, *Phys. Rev.* **1955**, *100*, 564.

[103] B. Henne, V. Ney, M. de Souza, A. Ney, *Phys. Rev. B* **2016**, *93*, 144406.

[104] L. Balents, *Nature* **2010**, *464*, 199.

[105] J. S. Gardner, M. J. P. Gingras, J. E. Greedan, *Rev. Mod. Phys.* **2010**, *82*, 53.

[106] E. Stavitski, F. M. F. de Groot, *Micron* **2010**, *41*, 687.

[107] J. Rodríguez-Carvajal, *Phys. B (Amsterdam, Neth.)* **1993**, *192*, 55.

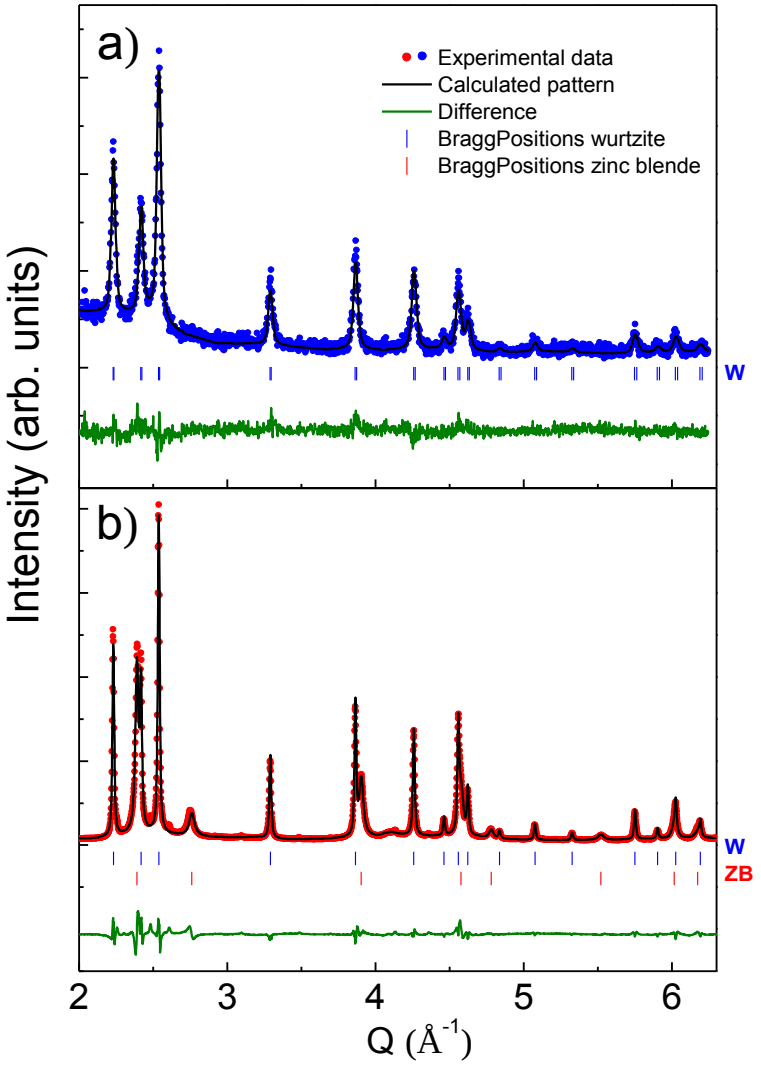

Figure 1. X-ray diffraction patterns of the (a) pure wurtzite and (b) mixed wurtzite – zinc blende CoO samples.

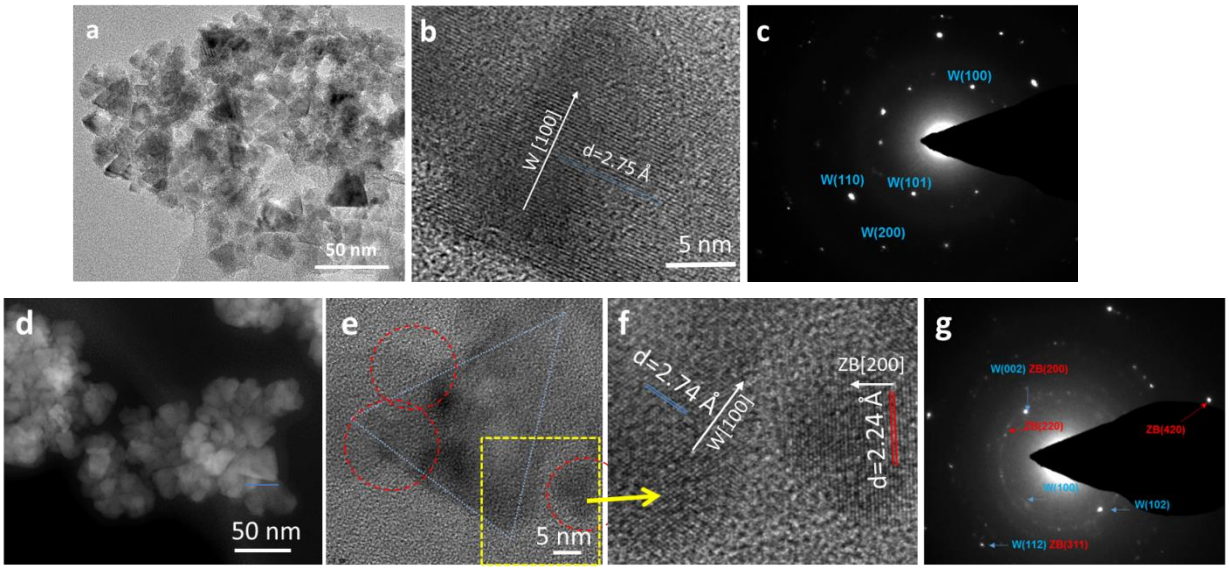

Figure 2. (a) TEM, (b) HR-TEM images and (c) SAED of the pure wurtzite-CoO sample. (d) Low resolution HAADF-STEM image (e) TEM image of a few nanoparticles, (f) HR-TEM image and (g) SAED of the mixed wurtzite-CoO and zinc blende-CoO sample.

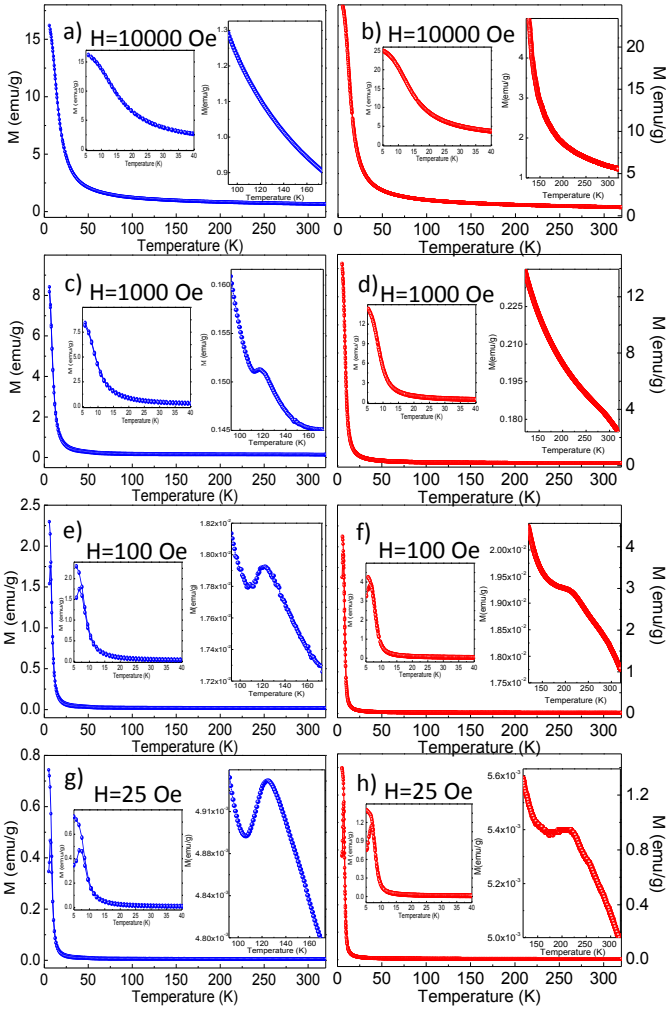

Figure 3. Temperature dependence of the field cooled and zero field cooled magnetization for (a, c, e, g) the pure wurtzite-CoO sample and (b, d, f, h) the mixed wurtzite–zinc blende CoO sample, measured at different applied fields: 25, 100, 1000 and 10000 Oe. Shown in the insets are enlarged areas of different temperature ranges.

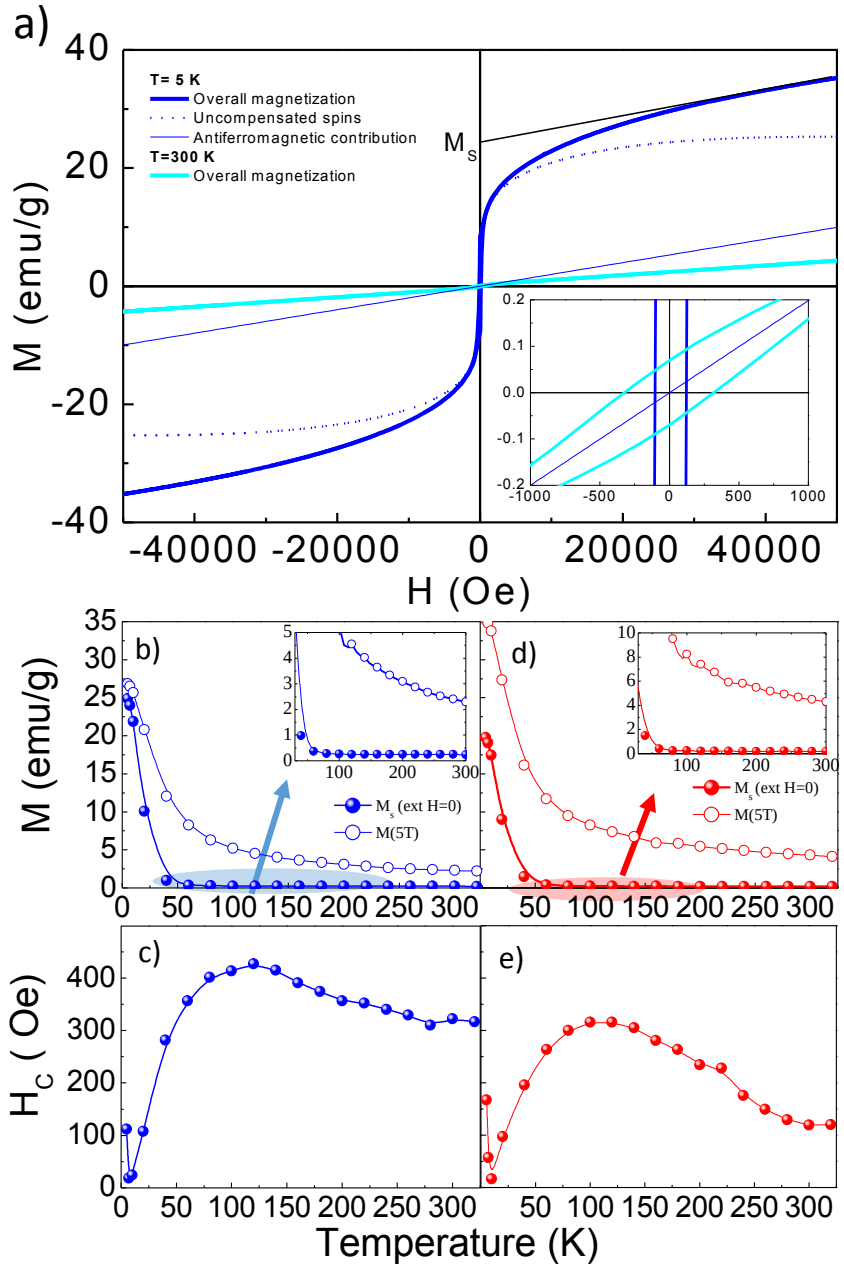

Figure 4. (a) Hysteresis loops of the pure wurtzite-CoO sample at 5 K (with AFM and uncompensated spin contributions disclosed) and 300 K. (b) and (d) show the temperature dependence of M_S [extrapolated to H = 0, M_S(ext H=0)] and the magnetization at H = 5 T [M(5T)] for the pure wurtzite and mixed wurtzite – zinc blende CoO samples, respectively. (c) and (e) display temperature dependence of H_C for the pure wurtzite-CoO and mixed wurtzite – zinc blende CoO samples, respectively.

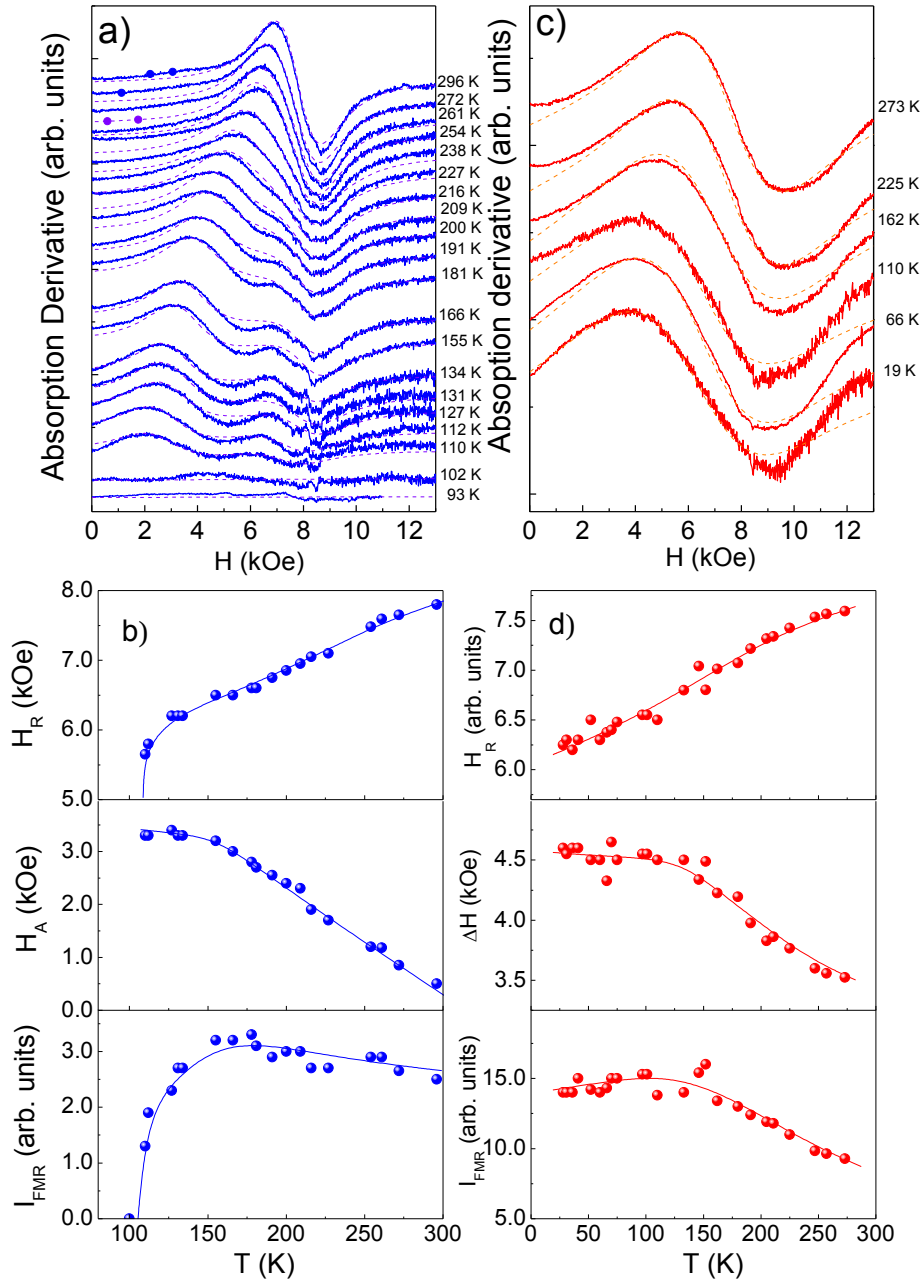

Figure 5. (a) and (c) show FMR spectra at different temperatures for the pure wurtzite-CoO and mixed wurtzite-zinc blende CoO samples, respectively. The spectra are vertically shifted for clarity. The solid lines correspond to the experimental data, while the dot lines are fits to the data. (b) and (d) display the temperature dependence of the intensity (I_{ESR}), anisotropy field (H_R)-or linewidth (ΔH)- and resonance field (H_R) for pure wurtzite-CoO and mixed wurtzite- zinc blende CoO samples, respectively. The lines in (b) and (d) are guides to the eye.

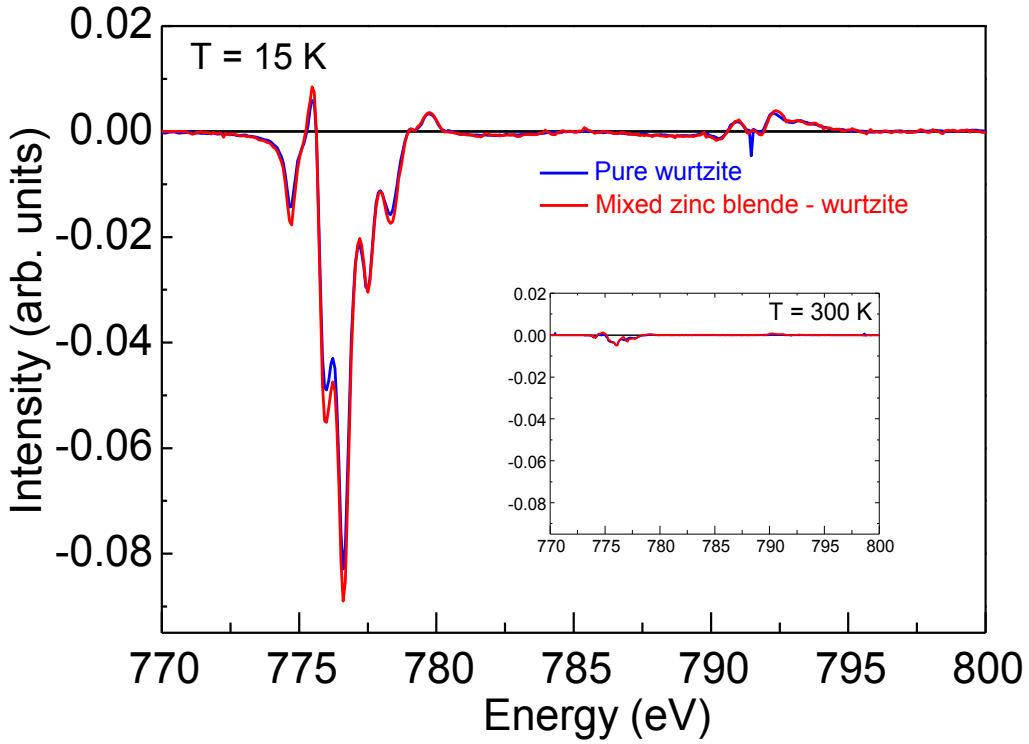

Figure 6. Co $L_{2,3}$-edge XMCD spectra at T = 15 K a for the the pure wurtzite (blue) and mixed wurtzite – zinc blende (red) CoO samples. Shown in the inset are the spectra at T = 300 K of the same samples.

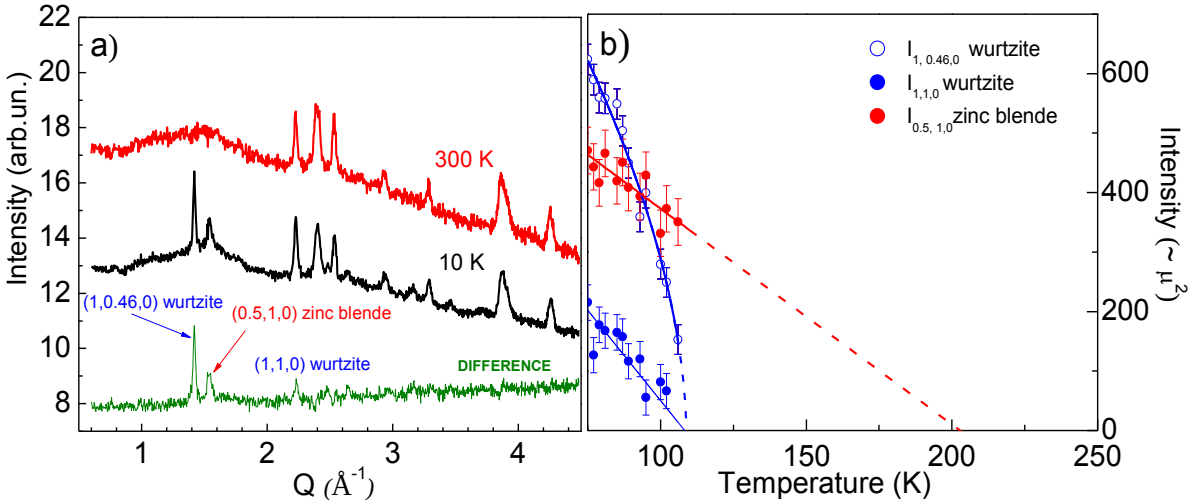

Figure 7. (a) Neutron diffraction patterns of the mixed wurtzite – zinc blende samples at 10 K (black) and 300 K (red) and their difference (green). Note that the patterns have been shifted for clarity. (b) Temperature dependence of (1, 0.46, 0)-incommensurate (empty blue symbols) and (1, 1, 0) (filled blue symbols) magnetic reflections from wurtzite-CoO and the (0.5, 1, 0) magnetic reflection from zinc blende-CoO (red symbols). The solid lines are fits of the power law $(T\text{-}T_N)^{2\beta}$, with β = 0.5 for wurtzite (110) and zinc blende (0.5, 1, 0) and β = 0.28 for wurtzite (1, 0.46, 0). The dashed lines are extrapolations of the $(T\text{-}T_N)^{2\beta}$ power law to higher temperatures.

CoO nanoparticles with zinc blende and wurtzite structures are found to be antiferromagnetic below T_N ~ 225 K and 109 K, respectively. Although the zinc blende phase has a conventional antiferromagnetic structure, the antiferromagentic order of the wurtzite phase is more complex with two orthogonal components (one of them incommensurate). The nanoparticles also present a large number of uncompenstaed spins.

Keywords: CoO wurtzite, CoO zinc blende, antiferromagnets, incommensurate structures, uncompensated spins

Unraveling the elusive antiferromagnetic order in wurtzite and zinc blende CoO polymorph nanoparticles

Alejandro G. Roca, IgorV. Golosovsky, Elin Winkler, Alberto López-Ortega, Marta Estrader, Roberto D. Zysler, María Dolors Baró, Josep Nogués**